Laser and Particle Beams (1998), *vol.* 16, *no.* 1, *pp.* 61–70
Printed in the United States of America

Formation of the X-ray line emission spectrum of excimer laser-produced plasmas

By A. MAGUNOV,* A. FAENOV,* I. SKOBELEV,* T. PIKUZ,* D. BATANI,** M. MILANI,** M. COSTATO,† A. POZZI,† E. TURCU,‡ R. ALLOT,‡ M. KOENIG,§ A. BENUZZI,§ F. FLORA,¶ AND A. REALE‖

*Multicharged Ions Spectra Data Center, Mendeleevo, 141570, Russia
**Dipartimento di Fisica, Università di Milano, V.Celoria 16, Milano, Italy
†Dipartimento di Fisica, Università di Modena, Italy
‡Rutherford Appleton Laboratory, Chilton, Oxon (U.K.)
§LULI, Ecole Polytechnique, France
¶Dipartimento Innovazione, CRE ENEA, Frascati, Italy
‖Dipartimento di Fisica, Università dell'Aquila, Italy

(Received 1 October 1996; Accepted 30 July 1997)

Time- and space-integrated emission spectra measurements have been performed in plasma produced by 308 nm wavelength XeCl laser radiation ($I_L = (4–10)\cdot 10^{12}$ W/cm^2, $\tau = 10$ ns) and by 248 nm wavelength KrF laser pulse train radiation ($I_L = 5\cdot 10^{15}$ W/cm^2, $\tau = 7$ ps, 16 pulses in train) on CF_2 plane target. Theoretical modelling of Lyman series and He-like ion resonance series of fluorine and its fit of experimental data show considerable differences in the absorption of laser radiation in the two plasmas.

1. Introduction

The considerable interest for the studies of plasma production processes by short wavelength ($\lambda_L < 500$ nm) laser pulse radiation is due to many different applications, for example the development of optimal drivers for inertial fusion (see, *e.g.*, Fabre *et al.* 1980, Koenig *et al.* 1992) and of intense X-ray sources for various applications, including modern biological studies (Turcu *et al.* 1990, 1994). Such wavelength region is interesting because of its higher conversion of laser power to plasma energy. However, there are not enough experimental data yet to give an adequate picture of plasma evolution during its interaction with short wavelength laser radiation.

In recent times, different spectroscopic methods have been developed to study the X-ray spectra of laser-produced plasmas. Some of them provide high spatial or temporal resolution with addition to the spectral one. Very often, space and time resolution are required for a quantitative understanding of laser-plasma experiments, especially in the nanosecond regime. Indeed, spectra obtained in this way are the most informative for the determination of plasma parameters versus the laser pulse characteristics. Among these diagnostic methods we recall, for example, that proposed by d'Etat *et al.* (1987) based on the study of space resolved complete H-like fluorine Lyman series originating from subcritical plasma electron densities.

However, in this paper we want to show that, with some approximations, even time- and space-integrated spectra obtained by simpler spectroscopic method can also give useful information about the features of plasma production processes if they are used in cooperation with theoretical and numerical modelling.

 0263-0346/98 $12.50

In the present work, the X-ray spectra of resonance line series in H-like and He-like fluorine ions are considered. These spectra were obtained from the plasma produced by excimer XeCl laser radiation of the "Hercules" facility in Frascati and by KrF laser radiation at Rutherford Appleton Laboratory. The results of spectra modelling have allowed to see the differences of plasma formation in the subcritical region in these experiments even without spatial and temporal resolution.

2. Experimental set-up

The fluorine plasma spectra were obtained using two laser plasma production facilities, with quite different characteristics.

2.1. *Experimental set-up in Frascati*

The excimer laser used in Frascati is a ($10 \times 10 \times 100$ cm^3) discharge pumped XeCl system (wavelength 308 nm) named "Hercules," designed and built by ENEA, INN.FIS Department of Frascati (Bollanti *et al.* 1995). The capacitor bank of Hercules is directly connected with the laser electrodes, and a little before the rising voltage reaches the self-breakdown level an X-ray pulse is injected into the Ne-based XeCl gas mixture providing avalanche process. This photo triggering technique allows to circumvent the typical problem of having a reliable switching in the main discharge circuit. In this way, Hercules can be easily operated in the repetition rate mode, without limitations due to the both high charge transferred ($\approx$30 mC) and high current rate ($\approx 10^{11}$ A/s).

In this experiment, we used an injected PBUR (positive branch unstable resonator) configuration, which means that Hercules was used as a laser amplifier which amplified the beam produced by a Spectra Physics commercial laser with a 10 ns pulse duration. In this case, the obtainable energy was 2 J per pulse with 10 Hz repetition rate. Laser beam was focused by a triplet lens (with f-number $F = 3$) in 50–80 μm spots on the plane solid target to give an intensity $(4–10) \cdot 10^{12}$ W/cm^2.

2.2. *Experimental set-up at RAL*

The basic experimental arrangement is similar to the one described by Turcu *et al.* 1994. The laser system contains four modules:

a. *Oscillator.* It consists of a synchronously pumped modelocked dye laser oscillator. It gives a near diffraction limited laser beam with pulses of 5 ps duration and 1 nJ energy at 746 nm. The pumping system is a modelocked YAG at 82 MHz converted to second harmonic.

b. *Dye amplifier and frequency conversion.* There are two dye amplifier (one with double passage) pumped with a XeF excimer laser and two frequency conversion crystals working at 2ω and 3ω. The output is a 5 ps, 20-nJ pulse at 248 nm. The effect of frequency conversion are of getting the right wavelength which can be amplified in a final high power (excimer) amplifier and of reducing the pedestal of the picosecond pulse.

c. *Multiplexer.* It consists of a set of mirrors and beam splitters which forms a pulse train by splitting the original pulse in about 20 pulses (5 ps each) separated by 2 ns.

d. *Final amplifier.* It is a double pass KrF excimer laser which gives a final output with the following main characteristics: wavelength 248 nm, pulse train made of about 16 pulses (7 ps each) separated by 2 ns, total energy delivered by one pulse train about 300 mJ. While the oscillator works at MHz repetition frequency, both excimer lasers (XeF and KrF) work at a repetition frequency of a few tents Hz.

The beam was focused with a $f = 9$ cm lens to give an intensity on target $5 \cdot 10^{15}$ W/cm^2. All spectra collected during the experiment were taken working at a 20 Hz laser firing repetition rate.

2.3. *X-ray spectra detection*

The target was a thin TEFLON (CF_2) film (100 μm thickness). The X-ray spectra of H-like and He-like fluorine plasma were detected with the same spectrograph (which is described in Batani *et al.* 1991) in both cases. The experimental scheme is shown in figure 1. The Bragg mini-spectrometer was equipped with a RbAP crystal (2d = 26.121 Å). Plasma radiation was filtered with 3 μm Al and 2 μm paralyne and recorded on Kodak DEF films. Deconvolution of spectra took into account film calibration (Rockett *et al.* 1985), spectrometer geometry, and filter transmissivity.

3. Interpretation and modelling of plasma spectra

The geometry of plane crystal Bragg spectrometer (see figure 1) provides the spectral emission probability estimated from the experimental data to be presented in the form

$$P(E) = \frac{1}{4\pi} \iint Q_E(\mathbf{r},t) e^{-\tau_E(r,n_E,t)}\, d\mathbf{r}\, dt \tag{1}$$

with

$$\tau_E(\mathbf{r},\mathbf{n},t) = \int_S^\infty k_E(\rho + \mathbf{n}s',t)\, ds'$$

where E is the photon energy, $\mathbf{n}_E$ is the Bragg angle direction of photon emitted in point $\mathbf{r} = \rho + \mathbf{n}_E S$. The emissivity $Q_E(\mathbf{r},t)$ and the spectral absorption coefficient $k_E(\mathbf{r},t)$ depend on local plasma electron density $N_e(\mathbf{r},t)$, temperature $T_e(\mathbf{r},t)$ and ion charge abundance. In the case under consideration

$$Q_E(N_e,T_e) = 6.58\cdot10^{-16} \sum_n A_{n1} S_{n1}(E) N_n(N_e,T_e) + Q_E^{ph}(N_e,T_e) \tag{2}$$

and

$$k_E(N_e,T_e) = 2.53\cdot10^{-24} E^{-2} \sum_n A_{n1} S_{n1}(E) g_n N_1 \tag{3}$$

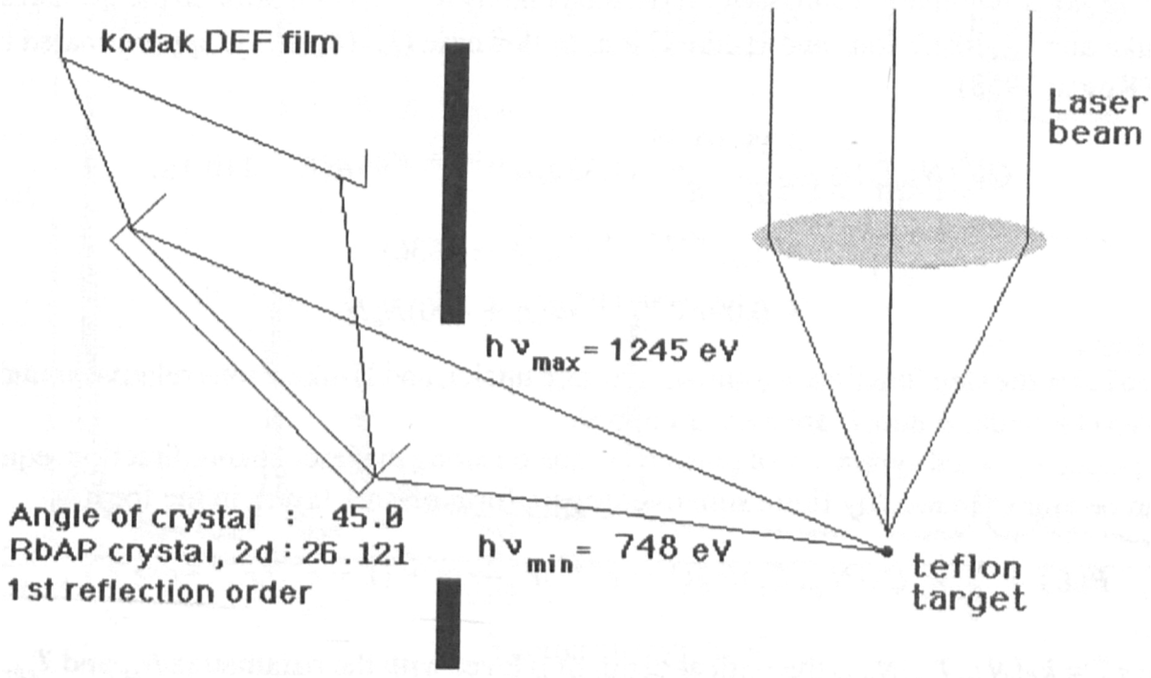

FIGURE 1. The X-ray spectrograph scheme in the experiments. The only difference was in the position of plasma radiation source. The RbAP crystal with 2d = 26.121 Å was used.

where A_{n1} is the radiative transition rate $np \rightarrow 1s$, N_n and N_1 is the upper and ground level population respectively, g_n is the level statistic weight, $S_{n1}(E)$ is the normalized line profile function for E measured in eV, and $Q_E^{ph}(N_e,T_e)$ describes the photorecombination continuum, while the bremsstrahlung emission is negligible. The sum is going on H-like and He-like line series.

The line profiles for H-like F IX can be derived taking into account quasistatic ion microfield Stark broadening, electron elastic collision, and Doppler broadening in the form (see Derzhiev *et al.* 1985 for details)

$$S_{n1}(E) = \sum_n \frac{\gamma_{n\alpha}}{\Delta E_n^D \sqrt{\pi}} \int_0^\infty W\left(\frac{E - E_{n1} - \Delta E_{n\alpha}^S \beta}{\Delta E_n^D}, \frac{\Delta E_{n\alpha}^c}{\Delta E_n^D}\right) P_a(Z_i,\beta)\, d\beta \tag{4}$$

here $\gamma_{n\alpha} = A_{n\alpha 1}/A_{n1}$ is the relative transition probability for the sublevel with parabolic quantum numbers $\alpha \equiv (n_1,n_2,m)$, $W(x,y)$ is the Voigt function for collision width $\Delta E_{n\alpha}^c(N_e,T_e)$ (Griem 1974) and Doppler width $\Delta E_n^D(T_e + T_d)$ with the effective temperature T_d corresponding to the mean expansion velocity, $\Delta E_{n\alpha}^S$ is the linear Stark shift of the sublevel in the field $F_0 = Z_i e/r_0$ with mean separation between ions $r_0 = 0.62 N_i^{-1/3}$, Z_i and N_i are the mean charge and density of the ions. The ionic microfield $F = F_0\beta$ probability distribution function $P_a(Z_i,\beta)$ with $a = r_0/r_D$, where r_D is the electron Debye radius, accounts for electron screening and ion correlation effects (Tighe & Hooper 1976).

We assume that equation (4) is valid for the resonance transition from $n \geq 4$ levels of the He-like fluorine (Bethe and Salpeter 1957), since the relativistic effects and electron interaction are small compared with the perturbation by the ionic microfield and Doppler line shift in the electron density range

$$10^{19} T_D^{3/4} Z^{13/4} n^{-3} \leq N_e \leq 8 \cdot 10^{23} Z^4 n^{-15/2}\ \text{cm}^{-3} \tag{5}$$

where $T_D = T_e + T_d$ (measured in kilo-electron-volts). The upper limit is determined by the overlapping of neighboring lines of the series (Inglis & Teller 1939). For $1s2p \rightarrow 1s^2$ and $1s3p \rightarrow 1s^2$ transitions, the Coulomb approximation is worse for the central part of line profiles. However, in optically thick plasma, the line widths for these transitions are defined by Stark wings where the ionic microfield effects still dominate.

The photorecombination emissivity is defined mainly by recombination to the ground states of H-like and He-like F ions and H-like C ion. In this case $Q_E^{ph}(N_e,T_e)$ is approximated in the form (Kogan 1958)

$$\begin{aligned} Q_E^{ph}(N_e,T_e) = \frac{4.25 \cdot 10^{-24}}{T_e^{3/2} E} & \left(1.35 a_N e^{(1101.6-E)/T_e} \theta(E - 110.16)\right. \\ & + \alpha_H e^{(953.6-E)/T_e} \theta(E - 9536) \\ & \left. + 0.09 e^{(490-E)/T_e} \theta(E + 490) N_e N_i \right) \end{aligned} \tag{6}$$

where $\theta(x)$ is the step function, α_N and α_H are bare nuclei, and H-like F ions relative abundance respectively, while E and T_e are measured in eV.

Proposing the axial symmetry of plasma expansion along the laser beams direction, equation (1) can be approximated by finite sum over the uniform plasma layers in the form

$$P(E) = \sum_p w_p Q_E(N_{ep},T_{ep})/\tau_E^p (1 - e^{-\tau_E^p}) e^{-\sum_{p'>p} \tau_E^{p'}} (1 + e^{-\tau_E^p} e^{-2\sum_{p'<p} \tau_E^{p'}}) \tag{7}$$

where $\tau_E^p = k_E(N_{ep},T_{ep}) R_p$ is the optical depth of p layer with the parameters N_{ep} and T_{ep}, R_p is the time- and space-averaged size of uniform plasma layer, and w_p gives the time- and space-integrated weight for corresponding plasma parameters. The electron density decreases mo-

notonously from the symmetry axis ($N_{ep} < N_{ep}$, for $p > p'$). Different multipliers in equation (7) account for the absorption of radiation in internal and external plasma regions and by uniform layer itself. In the case of optically thin plasma equation (7) reduce to

$$P(E) = \sum_p w_p Q_E(N_{ep}, T_{ep}). \tag{8}$$

The values w_p and R_p in (7) can be treated as adjusted parameters, while emissivity and absorption coefficient can be derived from plasma modelling.

In summary, our analysis has the following main characteristics:

1. it is based on the analysis of line spectra, rather than continuum,
2. it takes into account the effect of plasma opacities in the uniform multilayer approximation (equation 7) where the optical depth is calculated by equations 3 and 4 with the sizes R_p of the plasma layers are adjusted by best fit to the experimental data;
3. it is a stationary analysis whose validity could be questioned in the case of the short pulse KrF laser. While we want to show that already such stationary analysis can evidence many differences in the interaction of the laser with the plasma, this defect is easily removable by coupling with a hydrodynamic code.

4. Results and discussion

Figures 2–4 present spectra obtained in Frascati and RAL experiments. We start with the modelling of F IX and F VIII resonance series spectra obtained on Hercules facility. As was shown in earlier measurements of Na plasma spectra with spatial resolution (Faenov *et al.* 1996), the laser radiation of low intensity $I_L < 10^{13}$ W/cm^2 is absorbed in subcritical plasma region in agreement with the theoretical model of Mora (1982). In the case of XeCl radiation,

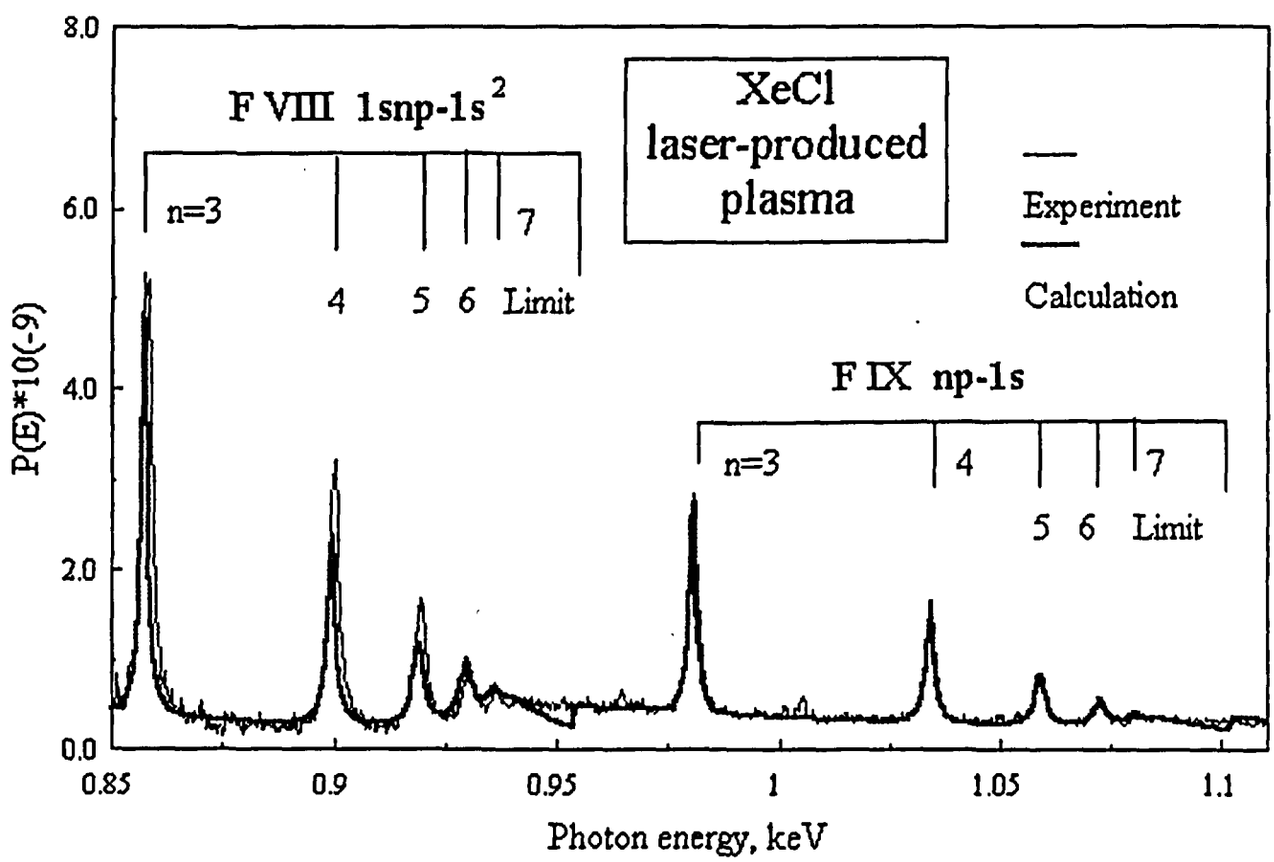

FIGURE 2. Experimental and theoretical F IX and F VIII spectra emitted from XeCl laser-produced plasma. Spectral region of *np*-1s transitions with $n \geq 3$ is shown.

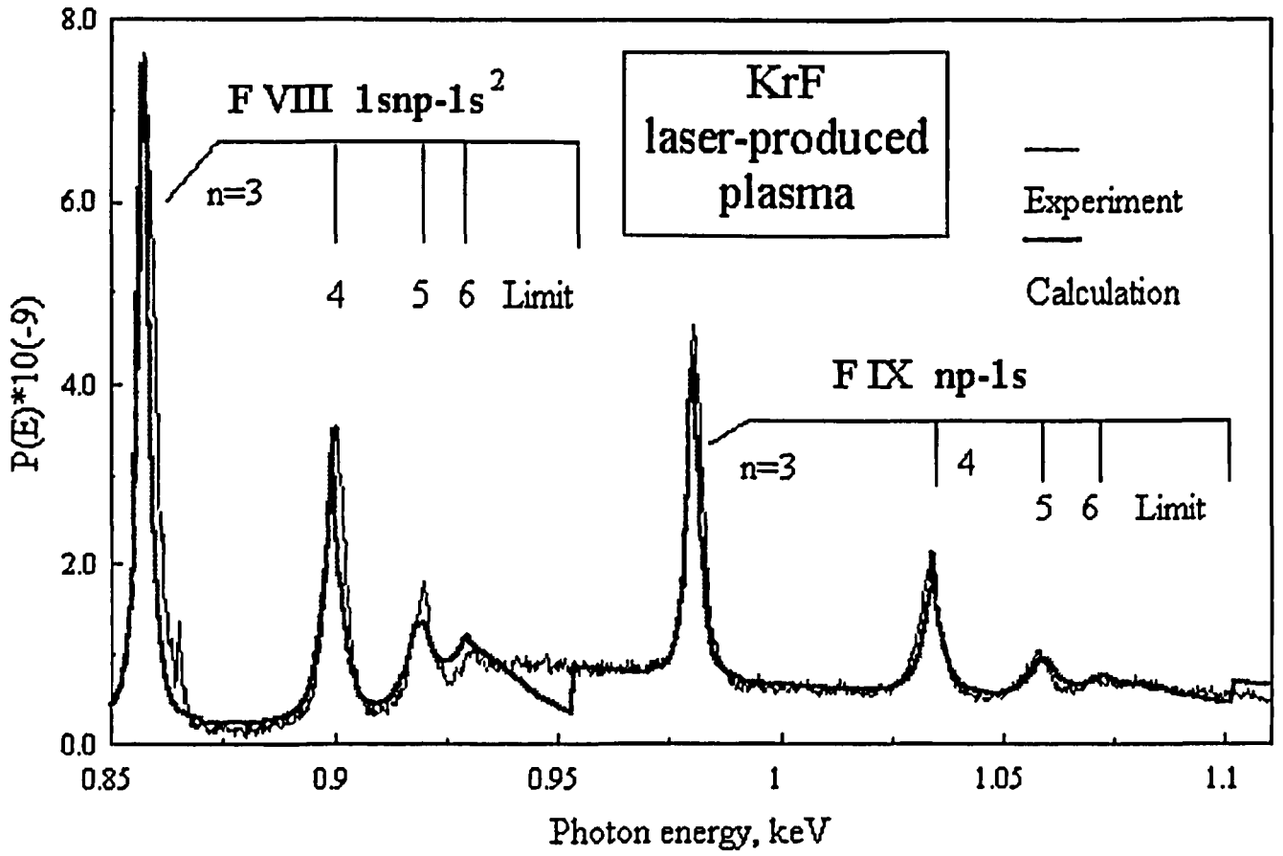

FIGURE 3. The same as in figure 2, but for KrF laser-produced plasma.

it is the region with $N_e \approx N_{ec} = 10^{22}$ cm^{-3}. The Ingles-Teller criterion in equation (5) gives for N_{ec} the maximal resolved line in H-like series of F IX with $n = 5$.

The observation of higher n members of series in the experimental spectrum, shown in figure 2, confirms the contribution of lower density regions either during laser radiation absorption or expansion period of plasma evolution. The observation of 6p → 1s line of Lyman series corresponds to $N_e < 2.5 \cdot 10^{21}$ cm^{-3}. The 7p → 1s line of H-like F IX and $7\,^1P_1 \rightarrow 1\,^1S_0$ line of He-like F VIII are also pronounced in experimental spectrum that corresponds to electron densities $N_e < 1.5 \cdot 10^{21}$ cm^{-3}. As if the Lyman line is less intense, the abundance of bare fluorine ions in plasma has to be much smaller at these densities. The absence of $8\,^1P_1 \rightarrow 1\,^1S_0$ line of F VIII ion gives the low limit of plasma electron densities ($N_e \approx 5.5 \cdot 10^{20}$ cm^{-3}) that contribute to the integral spectrum. High density region ($N_e > 10^{22}$ cm^{-3}) gives the photorecombination continuum in the vicinity of Ly_α and $2\,^1P_1 \rightarrow 1\,^1S_0$ lines (see figure 4a) due to carbon ions [third term in equation (6)]. Relatively low recombination in F ions provides $\alpha'_N 1$ and $\alpha'_H 1$ for these densities and hence much lower electron temperature.

According to earlier remarks, we defined six electron density ranges with mean values $N_{ep} = 2 \cdot 10^{22}$, 10^{22}, $5 \cdot 10^{21}$, $2 \cdot 10^{21}$, 10^{21}, and $5 \cdot 10^{20}$ cm^{-3} for the experimental spectra modelling according to equation (7). The adjusting parameters were the weighting factors w_p and layer size values R_p. The F ion charge abundance was also varied to give correct relative intensities for F IX and F VIII lines. The carbon component was considered as completely stripped. The level population values were calculated in the stationary collisional-radiative model and were obtained to be in thermodynamic equilibrium with the continuum for excited states with $n \geq 3$. The stationary population for $n = 2$ levels had to be decreased to fit the experimental intensities for these lines.

Spectral line profiles for $n \leq 15$ of both F IX and F VIII ions series were calculated according to equation (4) to produce the complete spectrum. The blue wings of high n lines were truncated on the ionization threshold accounting for field ionization (d'Etat *et al.* 1987). The results

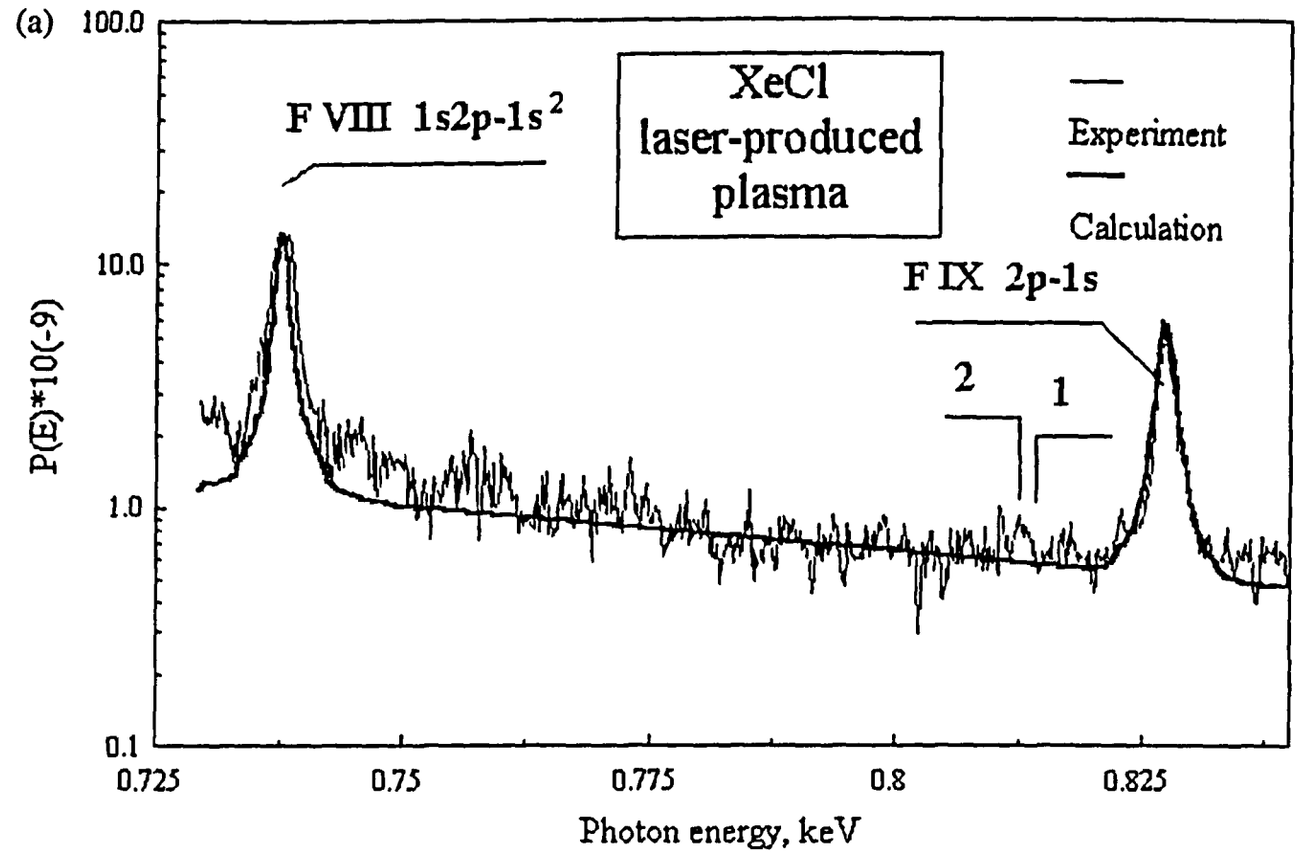

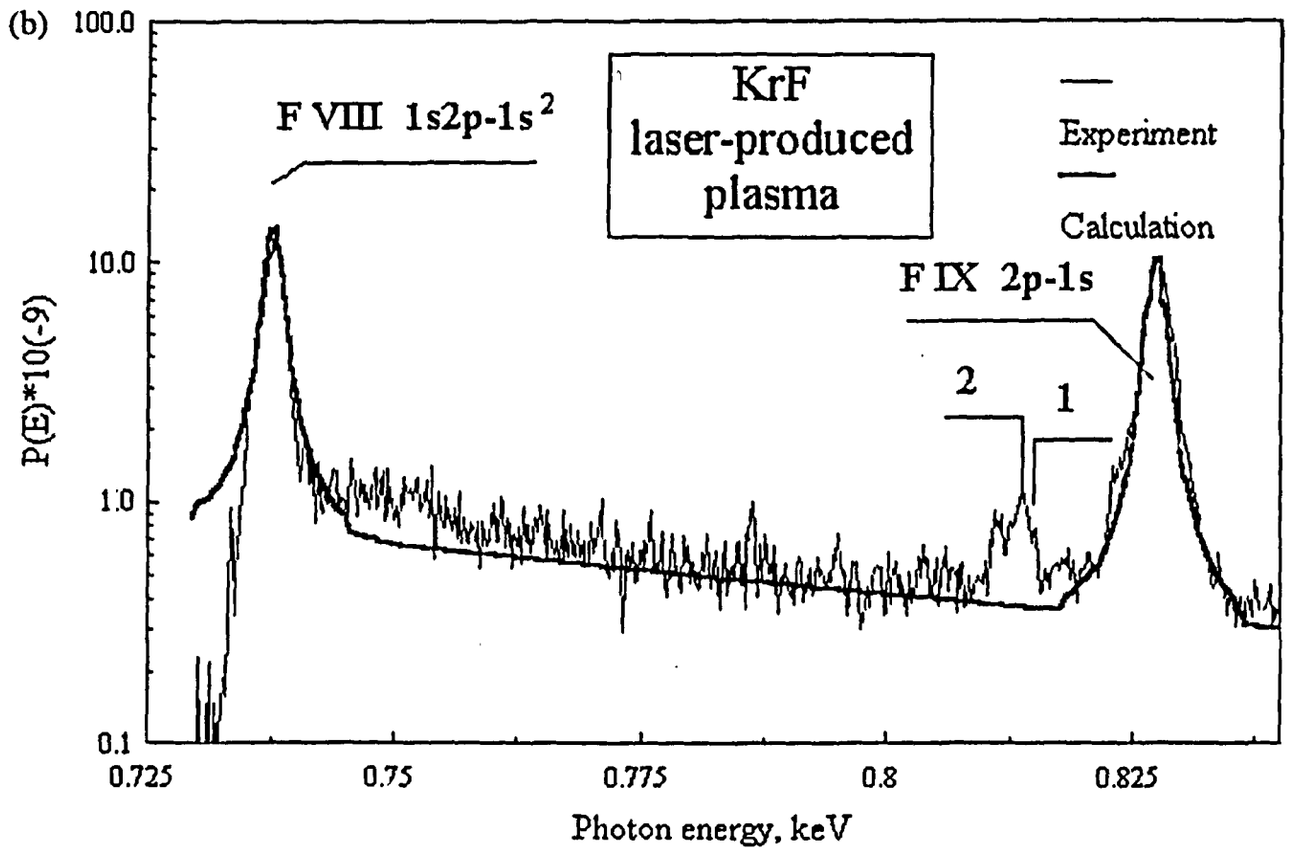

FIGURE 4. Experimental and theoretical spectra in the region of fluorine Ly_α, 2^1P_1–1^1S_0 and He-like satellites of Ly_α lines emitted from: (a) XeCl laser-produced plasma, (b) KrF laser-produced plasma. Satellite groups: 1–$2s2p\ ^3P_J \rightarrow 1s2s\ ^3S_1$ ($J = 0,1,2$), 2–$2p^2\ ^3P_J \rightarrow 1s2p\ ^3P_{J'}$, ($J,J' = 0,1,2$).

of fitting procedure are shown in figures 2 and 4a. The values of w_p parameters give correct line width for high members of series, and together with the ion abundance, provide the relative line intensities and photorecombination continuum of H-like and He-like ions. The R_p values determine the optical depth for each layer and thus the absorbed intensities of Ly_α and $2^1P_1 - 1^1S_0$ lines. Note that the electron temperature is less sensitive on the spectra and hence cannot be determined with the same accuracy. Indeed, the stationary kinetic modelling gives that the populations of the $n > 2$ levels are close to equilibrium with the continuum. In this case, line intensities are proportional to level statistic weights, and their ratio is almost independent of temperature (only through the Debye screening effect on line shapes and relative intensities through the level populations). Anyway, it was roughly estimated to be ≈200 eV for the Frascati experiment and ≈300 eV for the Rutherford case. Another method of measuring T_e would be through the slope of the continuum spectra at high photon energies. Values close to those previously reported are then obtained. Also for the continuum, we note that the photorecombination threshold is well evidenced in the theoretical curve while it is smoothed in the experimental one for some reason to be further investigated.

In the case of KrF laser-produced plasma, the critical density is slightly larger ($N_{ec} = 1.8 \cdot 10^{22}$ cm^{-3}). Such a difference could not change sharply the emission spectrum if the mechanisms of plasma formation were the same. However, the experimental data shown in figures 3 and 4b manifest the considerable differences in these spectra. First of all, the $7^1P_1 \rightarrow 1^1S_0$ line disappeared and lines with $n = 6$ in H-like and He-like series are much less pronounced than in the previous case. All lines are broader than would be according to simple scaling of the critical electron density.

These features confirm that in this case the laser radiation is absorbed in plasma layers that are close to critical region. Figure 5 presents the electron density dependence of weighting factors w_p provided the best fit for the two experiments. Clearly, the emission spectra of plasma produced by high intense KrF laser radiation is formed in much more dense plasma region near the critical electron density (see figure 5). Since inverse bremsstrahlung is the dominant absorption mechanism in both cases, this difference is likely to be due to the different pulse length

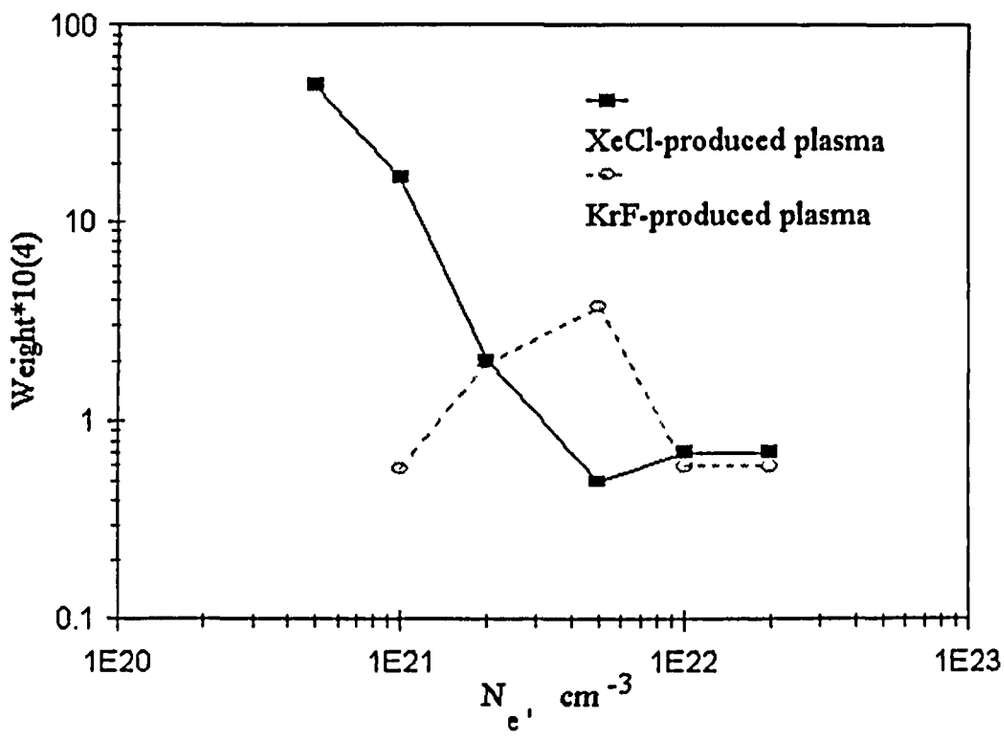

FIGURE 5. Electron density weight function from best fit of time and space integrated spectra of XeCl laser-produced plasma (solid curve) and KrF one (dashed curve).

which in the case of the psec KrF laser does not leave much time for the plasma to expand (and reach lower densities) during the laser pulse. Also, according to the already recalled Mora's model, absorption is delocalized if the laser intensity on target is $I_L < I_O$ where

$$I_O(\mathrm{W/cm^2}) = 2\cdot 10^{13}\lambda_L^{-5}(\mu\mathrm{m})(Z^*/3.5)^{-5}\tau^{1.5}\ (\mathrm{nsec}) \tag{9}$$

and Z^* is the average ionization degree in the plasma. Now, assuming $Z^* \approx 20$ as confirmed by our experimental X-ray spectra, it's easy to see that $I_L < I_O$ in the Frascati case (and hence absorption takes place at densities lower than critical) while $I_L > I_O$ in the Rutherford case (and hence absorption is practically at the critical density).

For determination of plasma electron density, we used also dielectron satellites caused by transitions from autoionizing states $2p^2\,{}^3P$ and $2s2p\,{}^3P$ of He-like F XIII ion. In the case of highly rarefied plasma (corona limit), dielectron capture causes predominant population of the $2s2p\,{}^3P$ levels, while the populations of the levels $2s2p\,{}^3P$ are small. With increasing density the levels $2p^2\,{}^3P$ are populated mainly by excitation from the levels $2s2p\,{}^3P$. Thus, the population ratio of $2p^2\,{}^3P$ and $2s2p\,{}^3P$ levels is density-sensitive in the region where the probability of collisional transition $2s2p\,{}^3P \rightarrow 2p^2\,{}^3P$ is the same order as the probability of noncollisional decay (radiative and autoionization) of $2s2p\,{}^3P$ states. In particular, level kinetic models (Vinogradov *et al.* 1977; Boiko *et al.* 1985) imply higher electron densities when satellite lines are more intense. For F VIII ions, this region is about $N_e \approx 10^{20}$–10^{22} cm^{-3}.

Radiative decay of the $2s2p\,{}^3P$ and $2p_2\,{}^3P$ levels leads to emission of seven high intense spectral lines with close wavelengths. A convenient (and sometimes the only possible) experiment procedure is to compare the total intensities of two groups of satellite lines (see figure 4)

1. $2s2p\,{}^3P_J \rightarrow 1s2s\,{}^3S_1$ $(J = 0,1,2)$
2. $2p^2\,{}^3P_J \rightarrow 1s2p\,{}^3P_{J'}$ $(J,J' = 0,1,2)$

Denoting the intensity ratio for these groups of lines by x and using the results of calculations (Seely 1981; Faenov *et al.* 1995), we obtain for the case of XeCl laser experiment $x_{\mathrm{exp}} = 1.15$ and $N_e = 3\cdot 10^{21}$ cm^{-3}, and for the case of KrF laser experiment $x_{\mathrm{exp}} = 1.4$ and $N_e = 8\cdot 10^{21}$ cm^{-3}.

5. Conclusion

Emission spectra of fluorine plasma produced by short wavelength excimer lasers radiation have been measured. The features of resonance series of H-like and He-like ions and the satellite lines were used for modelling, taking into account different spectral line broadening, population kinetics mechanisms, and radiative transfer. The best fitting of theoretical model results and experimental data for XeCl and KrF laser sources shows that time- and space-integrated spectra exhibit important differences in the interaction of laser radiation with plasma depending on laser pulse characteristics. The sensitivity of line emission spectra to the plasma parameters shows that the absorption efficiency of high intensity ($5\cdot 10^{15}$ W/cm^2) KrF laser radiation in plasma moves towards critical electron density region $N_e > 10^{22}$ cm^{-3}, while for much lower intensities (XeCl laser with $I_L < 10^{13}$ W/cm^2), the electron density region $N_e < 2\cdot 10^{21}$ cm^{-3} plays the main role.

Acknowledgments

Special thanks to Mr. C. Brown (RAL) for his invaluable help and patience and to Mr. G. Braga (Università di Milano) who has realized the Teflon tape. One of the authors (A.P.) thanks the Italian Physical Society (S.I.F.) for a grant. This work has partially been supported through the HCM "Access to Large Facilities" program and performed at Rutherford Appleton Laboratories, Chilton, Didcot, U.K. From the Russian side, this work was partly supported by Russian Fund of Fundamental Researches N 96-02-16111.

REFERENCES

BATANI, D. *et al.* 1991 *Excimer Lasers and Applications III* T Letardi Ed., SPIE vol. 1503.

BETHE, H.A. & SALPETER, E. 1957 *Quantum mechanics of one- and two-electron atoms* (Berlin-Springer), p. 245.

BOIKO, V.A. *et al.* 1985 *J. Sov. Laser Research* **6**, 85.

BOLLANTI, S. *et al.* 1995 *Physica Scripta* **51**, 326.

DERZHIEV, V.I. *et al.* 1985 *General Phys. Inst. Preprint* 56, Moscow (in Russian).

D'ETAT, B. *et al.* 1987 *J. Phys. B: At. Mol. Phys.* **20**, 1733.

FABRE, E. *et al.* 1980 *Plasma Phys. and Contr. Nucl. Fusion Research*, vol. II-IAEA-CN-38/I-4, Vienna.

FAENOV, A.YA. *et al.* 1995 *Phys. Rev. A* **51**, 3529.

FAENOV, A.YA. *et al.* 1996 *Kvantovaya electron* (*Quantum Electronics*), **26**, 701 (In Russian).

GRIEM, H.R. 1974 *Spectral line broadening by plasmas* (Academic, New York).

INGLIS, D.R. & TELLER, E. 1939 *Astrophys. J.* **90**, 439.

MORA, P. 1982 *Phys. Fluids* **25**, 1051.

KOENIG, M. *et al.* 1992 *Laser Particle Beams* **10**, 573.

KOGAN, V.I. 1958 *Fizika plasmi i problema upravlyaemih yadernih reaktsiy* M.A. Leontovich, ed. (Akademiya, Moscow), vol. 1, p. 99 (in Russian).

ROCKETT, P.D. *et al.* 1985 *Appl. Opt.* **24**, 2536.

SEELY, J. 1981 *Atom. Data and Nucl. Data Table* **26**, 137.

TIGHE, R.J. & HOOPER, C.F., JR. 1976 *Phys. Rev. A* **14**, 1514.

TURCU, E. *et al.* 1990 *Excimer Lasers and Applications II* T. Letardi, ed. SPIE vol. 1278, p. 32.

TURCU, E. *et al.* 1994 *Applications of Laser Plasma Radiation*, SPIE vol. 2015, p. 243.

VINOGRADOV, A.V. *et al.* 1977 *Sov. Phys. JETP* **45**, 925.